Comparative modelling of chemical ordering in palladium-iridium nanoalloys

Davis, Jack B A; Johnston, Roy L; Rubinovich, Leonid; Polak, Micha

DOI:
10.1063/1.4903188

Comparative modelling of chemical ordering in palladium-iridium nanoalloys

Jack B. A. Davis, Roy L. Johnston, Leonid Rubinovich, and Micha Polak

Citation: The Journal of Chemical Physics **141**, 224307 (2014); doi: 10.1063/1.4903188
View online: http://dx.doi.org/10.1063/1.4903188
View Table of Contents: http://scitation.aip.org/content/aip/journal/jcp/141/22?ver=pdfcov
Published by the AIP Publishing

Comparative modelling of chemical ordering in palladium-iridium nanoalloys

Jack B. A. Davis,[1] Roy L. Johnston,[1,a)] Leonid Rubinovich,[2] and Micha Polak[2,b)]
[1]*School of Chemistry, University of Birmingham, Birmingham B15 2TT, United Kingdom*
[2]*Department of Chemistry, Ben-Gurion University of the Negev, Beer-Sheva 84105, Israel*

(Received 1 October 2014; accepted 18 November 2014; published online 9 December 2014)

Chemical ordering in "magic-number" palladium-iridium nanoalloys has been studied by means of density functional theory (DFT) computations, and compared to those obtained by the Free Energy Concentration Expansion Method (FCEM) using derived coordination dependent bond energy variations (CBEV), and by the Birmingham Cluster Genetic Algorithm using the Gupta potential. Several compositions have been studied for 38- and 79-atom particles as well as the site preference for a single Ir dopant atom in the 201-atom truncated octahedron (TO). The 79- and 38-atom nanoalloy homotops predicted for the TO by the FCEM/CBEV are shown to be, respectively, the global minima and competitive low energy minima. Significant reordering of minima predicted by the Gupta potential is seen after reoptimisation at the DFT level. © *2014 AIP Publishing LLC*. [http://dx.doi.org/10.1063/1.4903188]

I. INTRODUCTION

Nanoalloys (NAs) are a class of nanomaterials composed of two or more metallic elements. These include nanoparticles (NPs), 2D-like structures, such as nanogrids and sheets, and 1D-like structures, such as nanowires and nanotubes.[1] For NA particles the combination of metals results in properties which are not only dependent on size and shape,[2] but also on the composition.[3] The presence of two or more elements introduces homotops, namely, isomers differing in only the ordering of atom types, increasing the complexity of the system's energy landscape.[4]

The combination of metals can increase the activity and/or the selectivity of catalysts.[3] This nanoalloying effect has been investigated theoretically[5] and experimentally[6–11] for the strongly demixing palladium-iridium system.[12–14] Pd–Ir NAs have been investigated for use in several catalytic processes, including the preferential oxidation of CO,[6,11] the selective hydrogenation of benzonitrile,[7] and tetralin hydroconversion, which is key to reducing particulate emissions arising from the combustion of diesel fuel.[8,9]

In order to rationalise the nanoalloying effect on the activity and selectivity of catalysts, their structural characterisation is essential. We have recently reported structures for 8-10 atom Pd–Ir clusters using global optimisation directly at the density functional theory (DFT) level.[5] This, however, is challenging for larger particles due to the computational expense of the local minimisation step and the larger initial search space.

A wide range of methods are available for the prediction of nanoalloy structures. These include basin hopping,[15] genetic algorithms,[16] and statistical mechanical methods.[17–19] The number of homotops rises combinatorially as the composition tends towards a 50/50 mixture, making the exploration of the energy landscape increasingly difficult.

The free energy concentration expansion method (FCEM) is a statistical mechanical approximation for the prediction of chemical ordering in NAs of up to 1000 atoms,[19,20] and beyond (Rubinovich and Polak, to be published). However, FCEM is limited to the prediction of the lowest energy homotop for a given crystalline structure only. The energetics required by FCEM can be provided by the extraction of coordination dependent bond energy variations (CBEV) from DFT computed surface energies.[21,22] The extension of FCEM/CBEV from central-symmetric to more complex chemical orderings has recently been reported for the study of Pt–Ir clusters.[23] The model was able to characterise "quasi-Janus" behaviour in the system, as has recently been investigated by Bochicchio and Ferrando.[24]

The goal of the present work is twofold: first, to study 0 K chemical ordering in Pd-Ir nanoalloys by means of DFT, and second, to compare it with results of the FCEM/CBEV and the Birmingham Cluster Genetic Algorithm (BCGA). The FCC truncated octahedron (TO) is chosen for Pd–Ir, as for larger clusters it can be assumed structures will replicate that of the bulk alloy.[12] Indeed, the TO has been found experimentally for Pd–Ir ∼3 nm NAs.[9] FCEM/CBEV calculations are performed for 38-, 79-, and 201-atom Pd–Ir magic-number TO structures.[1] Whilst the TO is probably not the lowest energy structure for the 38-atom NAs, these sizes were chosen because of the ability to assess the accuracy of FCEM/CBEV using DFT. If found to be reasonably accurate, confidence can be given to future studies on larger TOs, better suited to FCEM, which are not currently accessible to DFT-based methods.

The results for 38- and 79-atom particles are assessed through comparison to minima produced using the Birmingham Cluster Genetic Algorithm with the Gupta

a)r.l.johnston@bham.ac.uk
b)mpolak@bgu.ac.il

(BCGA/Gupta). All structures undergo further DFT local minimization for direct comparison. For the 201-atom TO, DFT calculations are carried out on all inequivalent structures to determine the favoured position of a single Ir dopant.

II. METHODOLOGY

A. Surface energies

The surface energies of Pd and Ir for six-surface orientations, (111), (110), (100), (311), (331), and (210) were calculated with DFT using the method of Methfessel.[25–27] Calculations were carried out with VASP,[28–31] using PAW pseudopotentials and the PBEsol exchange correlation (xc) functional.[32–34] A cutoff of 400 eV and Methfessel-Paxton smearing with a sigma value of 0.01 eV was used.[35] A k-point mesh of 19 × 19 × 1 was used for the slab calculations.[36] The bulk energies of Pd and Ir, E_{bulk}, were calculated using the same parameters but with a 3D 19 × 19 × 19 k-point mesh.

To construct the surface a large supercell was used.[37] The supercell consisted of a slab, made up of a certain number of atomic layers, and a vacuum spacing of around 20 Å between slabs. The number of layers required to replicate the surface properties was found by increasing the number of layers until the energy of the slab converged to 0.01 eV. Surface energies, σ, were then calculated using the energy of N atoms in the slab, E_{Slab}, and the bulk energy such that

$$\sigma = \frac{1}{2}(E_{Slab} - NE_{bulk}), \tag{1}$$

where the factor of 1/2 accounts for the two surfaces of the slab. The number of layers required to converge E_{Slab} was found to increase with the roughness of the surface. 14 layers were used for (111), 15 for (110) and (100), 21 for (311), and 32 for (331) and (210). The DFT computed lattice constants were used to construct the surfaces, 3.87 Å for Pd and 3.83 Å for Ir. The top and bottom three layers were allowed to relax during the DFT calculation.

B. FCEM/CBEV

FCEM is an efficient and reasonably accurate tool for the prediction of chemical ordering in alloys. Details of the expression for the free energy of a bimetallic NP can be found elsewhere.[19,20] For T = 0 K, energetic contributions (no entropic or short-range order terms) are given by

$$F = \sum_{p\le q} N_{pq} \left\{ \frac{1}{2} \sum_{I} w_{pq}^{II} \left(c_p^I + c_q^I\right) - \sum_{IJ} V_{pq}^{IJ} \left(c_p^I c_q^J + c_p^J c_q^I\right) \right\}. \tag{2}$$

The free energy is minimised with respect to the I-constituent concentrations, c_p^I, at all symmetry inequivalent sites, p, in a given structure, in this case a TO. Geometric input parameters include the number of nearest-neighbour pairs belonging to p and q sites, N_{pq}. Input energetic parameters include the elemental (homoatomic) pairwise interactions, w_{pq}^{II}, and the effective heteroatomic interactions, V_{pq}^{IJ}, between constituents I and J, $V_{pq}^{Ij} \equiv \frac{1}{2}\left(w_{pq}^{II} + w_{pq}^{JJ} - 2w_{pq}^{IJ}\right)$, obtained from their enthalpies of mixing.

For surface and subsurface sites coordination-dependent bond energy variations (CBEV, δw_{pq}) were extracted from DFT computed surface energies via[21,22]

$$\sigma = \sum_{p} \frac{1}{2} \left(\sum_{p(p\neq q)} \delta w_{pq} - \Delta Z_p w_b \right), \tag{3}$$

where w_b denotes the bulk bond-energy, $w_b = E_{bulk}/6$ (and $w_{pq} = w_b + \delta w_{pq}$). In particular, CBEV was approximated by a polynomial with coefficients fitted to (111), (110), (100), (311), (331), and (210) surface energies for each metallic element. For a $p - q$ pair bond with ΔZ_p and ΔZ_q broken bonds, δw_{pq} is considered as a function of symmetric, $x_{pq} = \Delta Z_p + \Delta Z_q$ and anti-symmetric, $y_{pq} = \Delta Z_p - \Delta Z_q$, coordination variables (y_{pq} takes into account the possible non-equivalence of two sites),

$$\delta w_{pq} = a_{1,0}x_{pq} + a_{2,0}x_{pq}^2 + a_{0,2}y_{pq}^2 \\ a_{3,0}x_{pq}^3 + a_{1,2}x_{pq}y_{pq}^2 + a_{4,0}x_{pq}^4. \tag{4}$$

In this way, energy variations are treated as coordination-dependent functions rather than numerical values. The implied basic assumption concerning the dominant effect of coordination, reflected in the use of common polynomials with element-specific coefficients, helps to circumvent transferability problems, namely, the need to repeat fitting of interactions for every site in a given nanoparticle surface structure.

In the present study, FCEM is expanded beyond only central symmetry equivalent sites.[23] For the TO the symmetry is relaxed and preserved along the [100] axis of the structure. For example, this increases the number of inequivalent sites from 4 to 10 in a 38-atom TO.

FCEM/CBEV calculations were performed using the FMINCON minimisation routine in MatLab. It can be noted that unlike the 0 K methods, FCEM/CBEV global minimum (GM) position was validated by smooth variations of site concentrations with decreased temperature.

C. Birmingham cluster genetic algorithm

Whilst possible for smaller systems,[38–40] the global optimisation of a 38-atom cluster at the DFT level is computationally challenging.[41–43] Another method of searching the DFT energy landscape is through the reminimisation of minima generated using a genetic algorithm and empirical potentials.[44,45] Unbiased BCGA calculations, using Gupta many-body atomistic potentials, were used to generate minima for Pd_4Ir_{34}, Pd_8Ir_{30}, $Pd_{20}Ir_{18}$, Pd_4Ir_{75}, and Pd_8Ir_{71}.[16,46] The 10 lowest energy structures were then selected.

The Gupta potential is based on the second moment approximation to tight-binding theory and is constructed from

TABLE I. Gupta potentials parameters for Pd–Pd, Ir–Ir, and Pd–Ir interactions.

$a-b$	Pd–Pd	Ir–Ir	Pd–Ir
A (eV)	0.175	0.116	0.145
ζ (eV)	1.718	2.289	2.004
p	10.867	16.980	13.924
q	3.742	2.691	3.217
r_0 (Å)	2.749	2.715	2.732

an attractive many-body term, V^m, and a repulsive pair term, V^r, summed over all N atoms[46]

$$V_{clus} = \sum_{i}^{N}[V^r(i) - V^m(i)], \tag{5}$$

where, for element types a and b and bond length r_{ij},

$$V^r(i) = \sum_{j\neq i}^{N} A(a,b)e^{(-p(a,b)(r_{ij}/r_0(a,b)-1))} \tag{6}$$

and

$$V^m(i) = \left[\sum_{j\neq i}^{N} \zeta^2(a,b)e^{(-2q(a,b)(r_{ij}/r_0(a,b)-1))}\right]^{1/2}, \tag{7}$$

where A, ζ, p, and q are parameters fitted to experimental values of the lattice parameters, experimental cohesive energies, and elastic constants at 0 K.[47] The Gupta parameters used are shown in Table I.

Spin-unrestricted calculations on the 10 minima and FCEM minima, using the same parameters as the surface energy calculations, were carried out using VASP. The geometry was allowed to relax in each case.

D. Energetics

Gupta binding energies, from BCGA calculations and stand-alone Gupta minimisations on FCEM structures, were calculated using

$$E_{b(Gupta)} = \frac{E}{N_{atoms}}, \tag{8}$$

where E is the total energy calculated from the Gupta potential and N_{atoms} is the total number of atoms in the NP. DFT binding energies were calculated using

$$E_{b(DFT)} = \frac{1}{N_{atoms}}[E_{A_nB_m} - nE_A - mE_B], \tag{9}$$

where $E_{A_nB_m}$ is the total energy of the particle and $E_{A/B}$ are the energies of the single atoms.

III. RESULTS AND DISCUSSION

A. Surface energies

The DFT computed surface energies for Pd and Ir are shown in Table II for both the relaxed, σ_r, and unrelaxed, σ_{ur}, surfaces that are consistent with those previously reported.[26,27,48,49] The relaxation of the surface is shown to make a considerable difference to σ and is, therefore, used for the derivation of δw_b. The CBEV polynomial coefficients derived for Pd and Ir are listed in Table III and the overall variations plotted in Figure 1. With respect to the bulk values, the strengthening of Ir–Ir bonds with decreasing coordination (increased $\Delta Z_1 + \Delta Z_2$) is consistently larger (i.e., δw is more negative) than for Pd–Pd bonds. This should result in some weakening of Pd surface segregation (via δw^{intra}) and should direct Ir to the subsurface (via δw^{inter}).

TABLE II. Unrelaxed, σ_{ur}, and relaxed, σ_r, energies, given in eV/(surface atom), of (111), (100), (110), (311), (331), and (210) surfaces for Pd and Ir. The corresponding bulk energies are also given.

		Pd		Ir	
	Layers	σ_{ur}	σ_r	σ_{ur}	σ_r
111	14	0.66	0.66	1.04	1.03
100	15	0.88	0.88	1.52	1.47
110	15	1.34	1.31	2.25	2.12
311	21	1.55	1.51	2.61	2.45
331	32	1.99	1.94	3.24	3.06
210	32	2.17	2.11	3.72	3.51
E_{bulk} (eV/atom)		−5.96		−9.81	

B. 38-atom NPs

The homotops predicted for the 38-atom TO by FCEM/CBEV for Pd_4Ir_{34}, Pd_8Ir_{30}, and $Pd_{20}Ir_{18}$ are shown in Figure 2. These all show Pd segregating on the (100) facets of the TO structure. Pd, which has a lower surface energy (shown in Table II),[50] preferentially occupies the lowest coordination sites. The formation of Pd–Pd bonds is favoured, preventing disruption of the stronger Ir–Ir bonds. This strong demixing tendency has been shown previously.[5]

VASP calculations were carried out on each of the structures predicted using the CBEV/FCEM method and the 10-lowest energy minima from BCGA/Gupta calculations. The results for Pd_4Ir_{34}, Pd_8Ir_{30}, and $Pd_{20}Ir_{18}$ are shown in Tables IV–VI, respectively.

At the DFT level the putative GM for Pd_4Ir_{34} is found to be BCGA minimum 1, an Ino-Decahedron (Ino-Dh) shown in Figure 3. Three of the Pd atoms in the structure are in low-coordinate dopant sites, minimising Ir–Ir bond disruption, as described by FCEM. The FCEM homotop is the overall second lowest energy structure and the lowest energy TO homotop, 4.41 meV/atom higher in energy than the GM. The

TABLE III. Values of the CBEV polynomial coefficients used for Pd and Ir.

Polynomial terms	Pd	Ir
$a_{1,0}$	2.36×10^{-2}	-4.13×10^{-2}
$a_{2,0}$	-1.46×10^{-2}	2.15×10^{-3}
$a_{0,2}$	8.94×10^{-3}	8.48×10^{-3}
$a_{3,0}$	3.48×10^{-4}	-1.47×10^{-3}
$a_{1,2}$	-1.35×10^{-3}	-1.37×10^{-3}
$a_{4,0}$	3.1×10^{-5}	8.59×10^{-5}

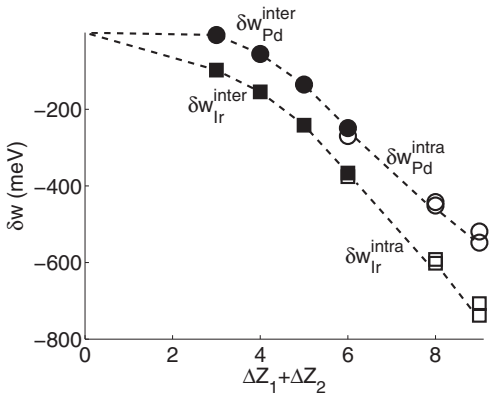

FIG. 1. The dependence on the number of broken bonds, $\Delta Z_1 + \Delta Z_2$, of surface-subsurface (filled symbols) and intrasurface (open symbols) bond-energy variations, δw, for elemental Pd (circles) and Ir (squares), as extracted from DFT-computed surface energies.

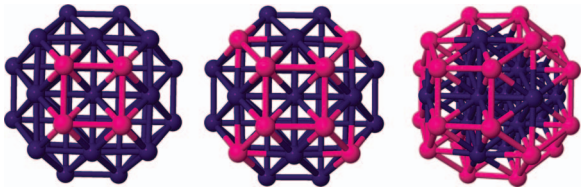

FIG. 2. Homotops predicted by FCEM/CBEV calculations for Pd_4Ir_{34}, Pd_8Ir_{30}, and $Pd_{20}Ir_{18}$, shown from left to right.

TABLE IV. Gupta and DFT binding energies, in eV/atom, and relative energies, in meV/atom, of FCEM and BCGA minima for Pd_4Ir_{34}.

	Structure	$E_{b(Gupta)}$	$E_{b(DFT)}$	ΔE_{Gupta}	ΔE_{DFT}
FCEM	TO	−5.3927	−6.2387	0.43	4.41
1	Ino-Dh	−5.3932	−6.2431	0.00	0.00
2	TO	−5.3929	−6.2288	0.24	14.29
3	TO	−5.3928	−6.2298	0.39	13.27
4	TO	−5.3926	−6.2293	0.57	13.87
5	Ino-Dh	−5.3923	−6.2328	0.86	10.34
6	TO	−5.3921	−6.2343	1.07	8.84
7	Ino-Dh	−5.3914	−6.2324	1.78	10.71
8	Ino-Dh	−5.3894	−6.2252	3.76	17.92
9	Ino-Dh	−5.3891	−6.2215	4.09	21.67
10	Ino-Dh	−5.3884	−6.2106	4.77	32.56

TABLE V. Gupta and DFT binding energies, in eV/atom, and relative energies, in meV/atom, of FCEM and BCGA minima for Pd_8Ir_{30}.

	Structure	$E_{b(Gupta)}$	$E_{b(DFT)}$	ΔE_{Gupta}	ΔE_{DFT}
FCEM	TO	−5.2044	−5.9216	19.73	1.92
1	Ino-Dh	−5.2241	−5.9221	0.00	1.46
2	...	−5.2204	−5.8998	3.65	23.76
3	...	−5.2202	−5.9023	3.86	21.24
4	...	−5.2175	−5.9108	6.55	12.69
5	...	−5.2169	−5.9235	7.21	0.00
6	...	−5.2168	−5.8833	7.33	40.22
7	...	−5.2165	−5.8761	7.59	47.40
8	...	−5.2147	−5.8994	9.40	24.13
9	...	−5.2138	−5.9065	10.29	17.08
10	...	−5.2136	−5.8869	10.45	36.62

TABLE VI. Gupta and DFT binding energies, in eV/atom, and relative energies, in meV/atom, of FCEM and BCGA minima for $Pd_{20}Ir_{18}$.

	Structure	$E_{b(Gupta)}$	$E_{b(DFT)}$	ΔE_{Gupta}	ΔE_{DFT}
FCEM	TO	−4.6421	−4.9817	0.00	2.00
1	TO	−4.6421	−4.9792	0.00	4.51
2	TO	−4.6419	−4.9781	0.19	5.57
3	TO	−4.6418	−4.9815	0.30	2.18
4	TO	−4.6415	−4.9798	0.63	3.86
5	TO-defect	−4.6301	−4.9837	12.01	0.00
6	Inc-Ih	−4.6297	−4.9775	12.41	6.19
7	Inc-Ih	−4.6270	−4.9570	15.11	26.64
8	Inc-Ih	−4.6262	−4.9564	15.90	27.29
9	Inc-Ih	−4.6260	−4.9692	16.13	14.43
10	TO-defect	−4.6246	−4.9798	17.50	3.83

Pd–Pd bonding predicted by FCEM is also seen in the GM, with a bond formed between two capping Pd atoms. Minimum 6 is the third lowest energy structure, here the Pd atoms form bonds on two separate (100) facets of the structure.

The BCGA search for Pd_8Ir_{30} finds only Ino-Dh as low energy structures, the putative global minimum is shown in Figure 4 (see the supplementary material for the complete set of minima[51]). When minimised with DFT there is significant reordering of minima, as seen in Table V, with the FCEM TO homotop becoming the third lowest energy structure, 1.92 meV/atom above the GM. Most Ino-Dh become significantly less favourable than the FCEM TO homotop. The global minimum Ino-Dh again shows Pd–Pd bonds across (100) faces of the structure.

The Gupta landscape for $Pd_{20}Ir_{18}$ shows a larger variety of structures, including TO, capped TO and structures based on capped inc-Ih-Mackay (Inc-Ih), shown in Figure 5 (energies are listed in Table VI).

The overall DFT GM is minimum 5, a structure with a Pd atom removed from the TO and moved to a (100)-capping

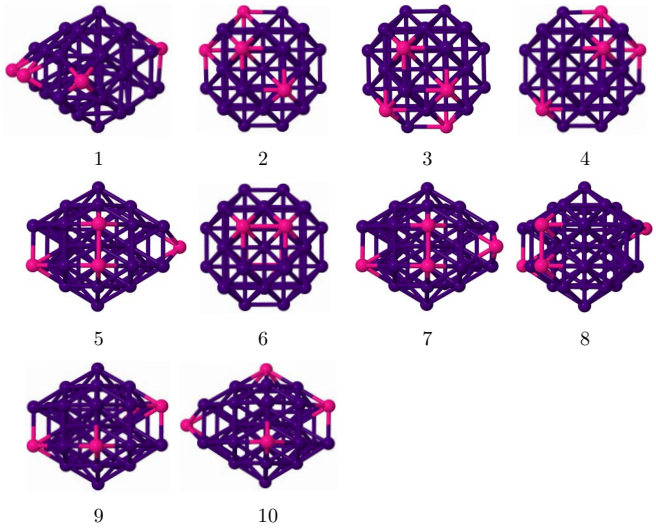

FIG. 3. Lowest energy structures from the BCGA search for Pd_4Ir_{34}.

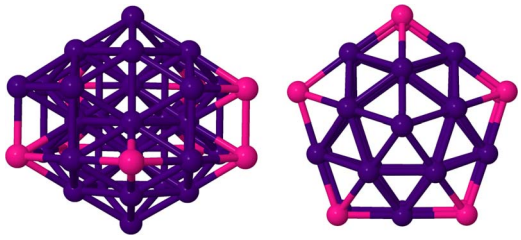

FIG. 4. Example of the Ino-Dh structure found for each BCGA minimum for Pd_8Ir_{30} (Minimum 1 in Table V is shown).

site. The formation of this vacancy allows the capping Pd to occupy a lower coordinate site, again preventing the disruption of Ir–Ir bonds. The FCEM homotop is the lowest energy complete TO structure found, 2 meV/atom above the GM.

C. 79-atom NPs

The homotops predicted for the 79-atom TO by CBEV/FCEM for Pd_4Ir_{75} and Pd_8Ir_{71} are shown in Figure 6. The predicted structures show Pd segregation towards the (100) facets of the TOs, as in the 38-atom case.

The results of DFT calculations on FCEM and BCGA minima, for Pd_4Ir_{75} and Pd_8Ir_{71}, are shown in Tables VII and VIII, respectively. In both cases, the FCEM TO predictions match perfectly the DFT GM and are much lower in energy than the Ino-Dh structures proposed by the BCGA, examples of which are shown in Figure 7 (see the supplementary material for the complete sets of minima[51]). This may be due to the difficulty the BCGA has in finding the GM. The search was repeated 100 times to ensure a higher probability of finding a low energy structure. The BCGA, however, may still struggle to search the systems conformational space efficiently. However, the $E_{b(Gupta)}$ values for Pd_8Ir_{71} show that the FCEM TO homotop is higher in energy than the BCGA minimum. The structure was therefore not missed by the search but discarded

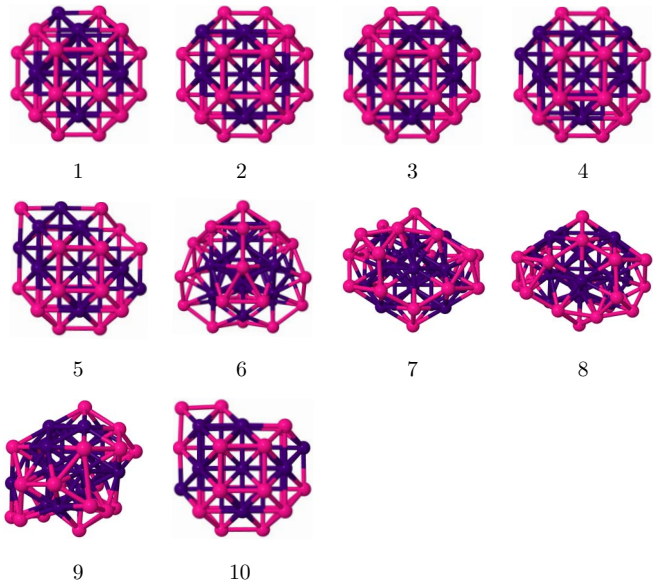

FIG. 5. Lowest energy structures from the BCGA search for $Pd_{20}Ir_{18}$.

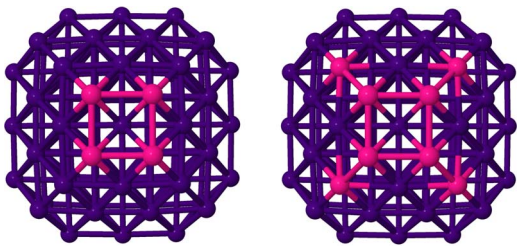

FIG. 6. Homotops predicted by FCEM/CBEV calculations for Pd_4Ir_{75} and Pd_8Ir_{71}.

TABLE VII. Gupta and DFT binding energies, in eV/atom, and relative energies, in meV/atom, of FCEM and the BCGA minima for Pd_4Ir_{75}.

	Structure	$E_{b(Gupta)}$	$E_{b(DFT)}$	ΔE_{Gupta}	ΔE_{DFT}
FCEM	TO	−5.7856	−6.9107	0.00	0.00
1	Ino-Dh	−5.7733	−6.8651	12.27	45.62
2	…	−5.7719	−6.8571	13.65	53.64
3	…	−5.7699	−6.8608	15.63	49.86
4	…	−5.7670	−6.8494	18.56	61.33
5	…	−5.7663	−6.8550	19.30	55.74
6	…	−5.7659	−6.8523	19.68	58.34
7	…	−5.7653	−6.8514	20.21	59.28
8	…	−5.7650	−6.8594	20.57	51.25
9	…	−5.7649	−6.8511	20.66	59.60
10	…	−5.7648	−6.8539	20.75	56.79

TABLE VIII. Gupta and DFT binding energies, in eV/atom, and relative energies, in meV/atom, of FCEM and the BCGA minima for Pd_8Ir_{71}.

	Structure	$E_{b(Gupta)}$	$E_{b(DFT)}$	ΔE_{Gupta}	ΔE_{DFT}
FCEM	TO	−5.6851	−6.7384	8.902	0.00
1	Ino-Dh	−5.6940	−6.7121	0.000	26.27
2	…	−5.6939	−6.7034	0.148	34.99
3	…	−5.6921	−6.7071	1.987	31.37
4	…	−5.6915	−6.7047	2.569	33.68
5	…	−5.6912	−6.6989	2.879	39.49
6	…	−5.6897	−6.7006	4.380	37.82
7	…	−5.6886	−6.7062	5.427	32.26
8	…	−5.6877	−6.7054	6.361	33.07
9	…	−5.6865	−6.6933	7.567	45.17
10	…	−5.6856	−6.7048	8.391	33.61

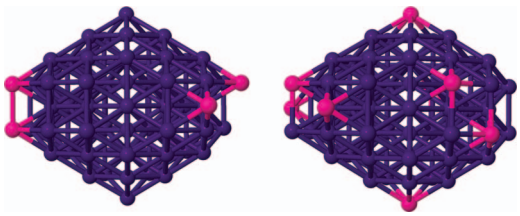

FIG. 7. Examples of Ino-Dh structures found for each BCGA minimum for Pd_4Ir_{75} and Pd_8Ir_{71} (putative global minimum 1 shown in each case).

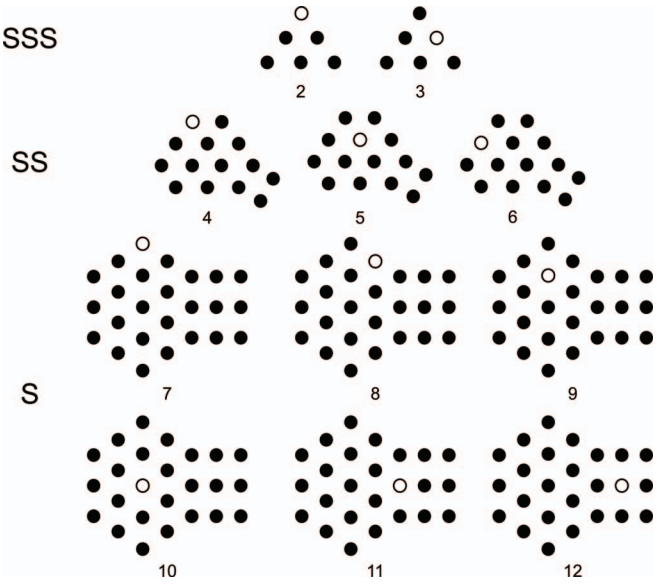

FIG. 8. Sites 2-12 from the sub-subsurface (SSS), subsurface (SS), and surface (S), shown from left to right, for the 201-atom TO (the central core site (1) is not shown).

because it is too high in energy. $E_{b(DFT)}$ shows that this predicted FCEM/CBEV structure is much more favourable at the DFT level.

D. 201-atom TO

The 201-atom TO has 12 different sites, shown schematically in Figure 8 (except for central site 1). To establish the site preference for a single Ir dopant atom in a 201-atom Pd TO, all inequivalent site binding-energies were assessed using DFT.[52] Due to both computational expense and the energetic cost of placing Ir on the surface, calculations were only carried out on only the first six sites, shown in Table IX.

Whilst DFT predicts the sub-subsurface site 2 to be the lowest energy, FCEM/CBEV predicts doping at subsurface site 4 to be lower in energy. It can be noted that the CBEV energetics can describe pair-wise interaction variations only at the surface and sub-surface of the NP.

TABLE IX. Binding energies for the 6 symmetry-inequivalent dopant sites of $Pd_{200}Ir$ TO.

Site	E_b (eV/atom)	ΔE (meV/atom)
1	−3.8789	1.53
2	−3.8802	0.00
3	−3.8797	0.51
4	−3.8798	0.42
5	−3.8797	0.53
6	−3.8799	0.34

IV. CONCLUSIONS AND FUTURE WORK

The DFT calculation of six surface energies for Pd and Ir has allowed extraction of CBEV parameters for the Pd–Ir FCEM computations. Through evaluation using the BCGA/Gupta and DFT calculations, the chemical ordering predictions made by FCEM/CBEV are shown to be quite accurate for both 38- and 79-atom Pd–Ir NAs. The model is either able to predict low energy minima or global minima, particularly in the 79-atom case.

Despite some limitations, FCEM/CBEV is based on analytical expressions, offering extremely quick calculations, which can include the temperature dependence and extraction of other thermodynamic properties. The present assessment of FCEM/CBEV can give confidence for calculations on system sizes significantly larger than the small NAs accessible to the more accurate current DFT-based methods (0 K).

FCEM/CBEV predictions for Pd–Ir NPs will serve as basis for the future study of the catalytic activity of this system. Initial work including the study of small molecule adsorption on the predicted structures is underway.

ACKNOWLEDGMENTS

J.B.A.D. and R.L.J. acknowledge the Engineering and Physical Sciences Research Council (EPSRC(U.K)) for funding under Critical Mass Grant No. EP/J010804/1 TOUCAN: Towards an Understanding of Catalysis on Nanoalloys. L.R. and M.P. acknowledge the Israel Science Foundation (ISF) (Grant No. 391/12). The authors thank COST action MP0903 for funding two short-term scientific missions.

Calculations were performed Via membership of the UK's HPC Materials Chemistry Consortium, which is funded by EPSRC (EP/L000202), this work made use of the facilities of HECToR and ARCHER, the UK's national high-performance computing service, which is funded by the Office of Science and Technology through EPSRC's High End Computing Programme.

[1] R. L. Johnston, *Atomic and Molecular Clusters* (Taylor and Francis, London, 2002).
[2] Y. Li and G. A. Somorjai, Nano Lett. **10**, 2289 (2010).
[3] R. Ferrando, J. Jellinek, and R. L. Johnston, Chem. Rev. **108**, 845 (2008).
[4] J. Jellinek and E. B. Krissinel, Chem. Phys. Lett. **258**, 283 (1996).
[5] J. B. A. Davis, S. L. Horswell, and R. L. Johnston, J. Phys. Chem. A **118**, 208 (2014).
[6] F. Morfin, S. Nassreddine, J. L. Rousset, and L. Piccolo, ACS Catal. **2**, 2161 (2012).
[7] Y. M. López-De Jesús, C. E. Johnson, J. R. Monnier, and C. T. Williams, Top. Catal. **53**, 1132 (2010).
[8] A. Rocha, E. Moreno, G. da Silva, J. Zotin, and A. Faro, Catal. Today **133–135**, 394 (2008).
[9] L. Piccolo, S. Nassreddine, M. Aouine, C. Ulhaq, and C. Geantet, J. Catal. **292**, 173 (2012).
[10] S. Shen, T. Zhao, and J. Xu, Electrochim. Acta **55**, 9179 (2010).
[11] C. Zlotea, F. Morfin, T. S. Nguyen, N. T. Nguyen, J. Nelayah, C. Ricolleau, M. Latrochea and L. Piccolo, Nanoscale **6**, 9955 (2014).
[12] S. N. Tripathi, S. R. Bharadwaj, and M. S. Chandrasekharaiah, J. Phase Equilib. **12**, 603 (1991).
[13] P. Turchi, V. Drchal, and J. Kudrnovský, Phys. Rev. B **74**, 064202 (2006).
[14] B. Kolb, S. Müller, D. Botts, and G. Hart, Phys. Rev. B **74**, 144206 (2006).
[15] D. J. Wales, and J. P. K. Doye, J. Chem. Phys. **101**, 5111 (1997).
[16] R. L. Johnston, Dalton Trans. **2003**, 4193.

[17]J. M. Montejano-Carrizales and J. L. Morán-López, Surf. Sci. **239**, 169 (1990).
[18]J. M. Montejano-Carrizales and J. L. Moran-Lopez, Surf. Sci. **239**, 178 (1990).
[19]M. Polak and L. Rubinovich, Surf. Sci. **584**, 41 (2005).
[20]L. Rubinovich, M. Haftel, N. Bernstein, and M. Polak, Phys. Rev. B **74**, 035405 (2006).
[21]L. Rubinovich and M. Polak, Phys. Rev. B **80**, 045404 (2009).
[22]M. Polak and L. Rubinovich, Int. J. Nanotechnol. **8**, 898 (2011).
[23]M. Polak and L. Rubinovich, Phys. Chem. Chem. Phys. **16**, 1569 (2014).
[24]D. Bochicchio and R. Ferrando, Phys. Rev. B **87**, 165435 (2013).
[25]M. Methfessel, D. Hennig, and M. Scheffler, Phys. Rev. B **46**, 4816 (1992).
[26]I. Galanakis, N. Papanikolaou, and P. H. Dederichs, Surf. Sci. **511**, 1 (2002).
[27]N. E. Singh-Miller and N. Marzari, Phys. Rev. B **80**, 235407 (2009).
[28]G. Kresse and J. Hafner, Phys. Rev. B **49**, 14251 (1994).
[29]G. Kresse and J. Hafner, Phys. Rev. B **47**, 558 (1993).
[30]G. Kresse and J. Furthmüller, Comput. Mater. Sci. **6**, 15 (1996).
[31]G. Kresse and J. Furthmüller, Phys. Rev. B **54**, 11169 (1996).
[32]P. Blöchl, Phys. Rev. B **50**, 17953 (1994).
[33]G. Kresse and D. Joubert, Phys. Rev. B **59**, 11 (1999).
[34]J. Perdew, A. Ruzsinszky, G. Csonka, O. Vydrov, G. Scuseria, L. Constantin, X. Zhou, and K. Burke, Phys. Rev. Lett. **100**, 136406 (2008).
[35]M. Methfessel and A. T. Paxton, Phys. Rev. B **40**, 3616 (1989).
[36]H. Monkhorst and J. Pack, Phys. Rev. B **13**, 5188 (1976).
[37]V. Fiorentini and M. Methfessel, J. Phys.: Condens. Matter **8**, 6525 (1996).
[38]C. J. Heard and R. L. Johnston, Eur. Phys. J. D **67**, 34 (2013).
[39]P. C. Jennings and R. L. Johnston, Comput. Theor. Chem. **1021**, 91 (2013).
[40]S. Heiles and R. L. Johnston, Int. J. Quantum Chem. **113**, 2091 (2013).
[41]X. Gu, S. Bulusu, X. Li, X. C. Zeng, J. Li, X. G. Gong, and L.-S. Wang, J. Phys. Chem. C **111**, 8228 (2007).
[42]N. Shao, W. Huang, Y. Gao, L.-M. Wang, X. Li, L.-S. Wang, and X. C. Zeng, J. Am. Chem. Soc. **132**, 6596 (2010).
[43]S. Bulusu, X. Li, L.-S. Wang, and X. C. Zeng, J. Phys. Chem. C **111**, 4190 (2007).
[44]R. Ferrando, A. Fortunelli, and R. L. Johnston, Phys. Chem. Chem. Phys. **10**, 640 (2008).
[45]L. O. Paz-Borbon, R. L. Johnston, G. Barcaro, and A. Fortunelli, J. Phys. Chem. C **111**, 2936 (2007).
[46]F. Cleri and V. Rosato, Phys. Rev. B **48**, 22 (1993).
[47]C. Kittel, *Introduction to Solid State Physics* (John Wiley and Sons, New York, 1986).
[48]L. Vitos, A. V. Ruban, H. L. Skriver, and J. Kollar, Surf. Sci. **411**, 186 (1998).
[49]J. L. Da Silva, C. Stampfl, and M. Scheffler, Surf. Sci. **600**, 703 (2006).
[50]W. R. Tyson and W. A. Miller, Surf. Sci. **62**, 267 (1977).
[51]See supplementary material at http://dx.doi.org/10.1063/1.4903188 for complete tables of minima discussed from the BCGA-Gupta searches.
[52]D. J. Wales, Chem. Phys. Lett. **285**, 330 (1998).